Controlled energy dispersion in two-dimensional decorated granular crystals

Luís Paulo Silveira Machado*
Universidade Federal do Pará, Brazil and Department of Physics, State University of New York, Buffalo, New York 14260-1500, USA

Surajit Sen†
Department of Physics, State University of New York, Buffalo, New York 14260-1500, USA

(Received 25 April 2018; published 28 September 2018)

The present study describes a way to control the dispersion of an impulse in a two-dimensional square granular crystal with tapered beads. The control is through the redirection of the characteristic load transfer path by controlling the shape of the scattering of wavefront. The main goal is to contribute to the development of appropriately designed granular media to mitigate impacts. The crystal is constituted of spherical granules with a wide range of radii. Interstitial particles are strategically positioned to allow a large number of collisions per unit area. The waves are produced by a striker that collides against the crystal. We analyze how material combinations, number of layers, tapering parameter, and disorder affect the decay of the wave amplitude. Our studies suggest that ∼90% impulse attenuation can be accomplished using a system thickness of 5 grains.

DOI: 10.1103/PhysRevE.98.032907

I. INTRODUCTION

There are several scenarios where it may be desirable to attenuate impacts. These include the protection of buildings against seismic shocks, vehicle surfaces, bullet proof vests, and areas to control explosions. Granular crystals are tunable, diverse, scalable, and simple systems where shock absorption features have been observed in a variety of studies. In fact, there is a growing literature even for 1D systems, where exhaustive reviews were reported by Sen *et al.* [1,2] and A. Rosas and K. Lindenberg [3]. One such family is the so-called decorated, tapered granular chains [4–6]. Chains are alignments of elastic spheres barely touching each other. Decoration is the inclusion of small spheres between larger spheres. While tapered chains are made with spheres that progressively shrink its radii. Many studies based on experiments [6–8], analytical methods [4–6,9–13], and simulations [14,15] have discussed the rapid dispersion of impulses and shock waves. Another important configuration is called the *granular container* [16–20]. It is a granular region built using monodispersed chains with different densities and different contact force laws. These aspects work together to effectively confine impulses.

However, arrays in 2D and 3D are natural candidates to provide better mitigation of propagating disturbances. A pioneering work by Shukla *et al.* [21,22] reported experimental and numerical investigations of wave propagation in a monodispersed chain, body-centered cubic arrangement, and hexagonal cubic arrangement using photoelastic disks. Extensive studies have shown the ability of granular media to redirect waves using proper arrangements [23–25]. Another series of works have shown how to change the shape of the wavefront using proper material combinations [26–28]. The influence of the number of layers, and post-impact movement for projectile impacting a 2D granular medium have also been studied [29]. More recently, a study of efficient dispersion in 2D arrangements showed significant attenuation of the incident energy [30]. While a study suggests the influence of interfaces between media in 3D with different densities [31]. There are rich possibilities in impact dispersion in 2D and 3D systems.

As we shall see, here we present a 2D decorated crystal that is different in the sense that unlike in previous studies, this system can accomplish remarkable impact dispersion using just a small number of layers. Hence, we believe that the current work may be useful in many contexts such as in making thin impact dispersion systems which may be useful in developing safer helmets. We numerically investigate the wave propagation in two-dimensional tapered granular systems subject to impulsive loading. Among issues addressed in this study are material combinations and how the tapering along the crystal improve the attenuation of the propagating momentum and energy. We close with some comments about disorder (random radii) and the angle of impact of the striker.

The paper is organized as follows: Sec. II details the granular arrangement, initial conditions, and the equations of motion. In Sec. III we discuss the dynamic response for the impact problem in a bidispersed and polydispersed granular system. Finally, Sec. IV presents a summary and description of continuing work.

II. MODEL

We study granular crystals as presented in Fig. 1. These arrangements are composed of two types of spherical granules: the *main granules* and *interstitial granules*. The main granules form a square array with the radii decreasing exponentially in each new layer. Similar to other works [11,13,15], the radii

*luismachado@ufpa.br
†sen@buffalo.edu

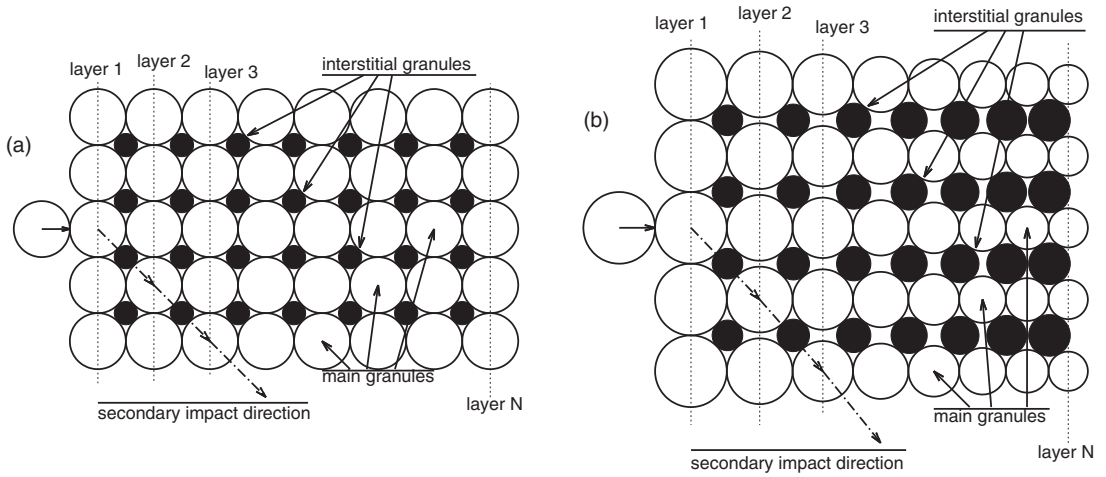

FIG. 1. Two-dimensional square arrangement constructed using two types of spherical granules: main and interstitial. The main granules form the square array and the interstitial granules are central particles strategically positioned in the interparticles spaces within the square array. There are no gaps and no pre-compression. Panel (a) and (b) correspond to $q = 0$ and 0.09, respectively, in Eq. (1). The striker is the only particle moving at $t = 0$. The secondary impact direction (SID) is a load transfer path to redirect the wave propagation from the impact line.

are given by

$$R_l = R(1+q)^{1-l}, \tag{1}$$

where R is the radius of the largest granules, q is the tapering parameter, and $l = 1, 2,..., N$ is the position of the layer in the crystal. The striker and those granules forming the first layer are the largest ones. All granules in each layer are identical. The main granules are primarily responsible for the perturbation propagation. The decrease in radii, and consequently the mass, is employed to help the momentum and force decay. These are expected behaviors that been observed in one-dimensional cases [7,8,11,13,15,32,33]. In addition, all granules can move freely at the crystal ends. We impose free boundary conditions at the edges.

The interstitial granules are extra granules with specific sizes and are strategically placed among the main granules to form a smaller array (see Fig. 1). The presence of interstitial granules should lead to no precompression and no gaps. To satisfy this scenario their radii increase according to

$$r_{l,l+1} = \frac{\sqrt{(2R)^2 + (R_l + R_{l+1})^2} - (R_l + R_{l+1})}{2}. \tag{2}$$

Note that all the interstitial granules between the l and $l+1$ layers are identical and they have the same radii. These extra granules are important to increase the number of particles per unit area. Among the main differences of the present arrangement is the inclusion of these localized non-uniformities in the medium. The dynamic response is expected to be comparable to what has been described in other studies [15]. The interstitial granules trap part of the perturbation (energy and momentum) in the form of vibration. The rest of the perturbation is dispersed (scattered) into other degrees of freedom along the system. The resultant system hence effectively mitigates waves.

However, as a consequence of how we position the granules, the number of layers forming the crystal must be limited to keep the crystal initially in the equilibrium state. Otherwise, there will be an overlap or precompression between the granules, i.e., initial local compressive forces in the contact lattice. A system like that has not been studied here. The number of layers is necessarily small by construction.

The crystals in Fig. 1 have the following initial conditions: the granules only touch each other, without precompression and without gaps, and all but the striker are at rest. The latter condition is responsible for imparting energy and momentum to the system that propagates as waves. The way those waves are scattered along the crystal is our central theme.

To model the time evolution we neglect the dissipation and rotation effects. We have observed that the influence of these effects are small for the wave dispersion in the present 2D crystal. Thus, the multiple elastic collisions in a very short crystal with high polydispersity are sufficient to reduce the wave amplitude. We model the interaction of ith granule when compressed against the jth granule following the Hertzian contact law. There is no interaction when the particles are separated. The equation of motion represents the granules, upon contact, as point masses interacting via nonlinear elastic springs [1–3,24] and can be written as

$$m_i \frac{d\mathbf{V}_i}{dt} = -\sum_j \alpha_{ij} (\delta_{ij}^{+})^{3/2} \hat{n}_{ij}, \tag{3}$$

where m_i, $\mathbf{V}_i$, and t are the mass, velocity vector, and time, respectively. The expoent $3/2$ is to model spheres. For disks or parallel cylinders the force is linear, with harmonic potential. The sum is performed over the neighbors of granule i, δ_{ij}^{+} is the normal compression between granule i and its neighbor j (see Fig. 1), and α_{ij} is the elastic coefficient described by

$$\alpha_{ij} = \frac{4 Y_i Y_j \sqrt{\frac{R_i R_j}{R_i + R_j}}}{3Y_i\left(1-\nu_j^2\right) + 3Y_j\left(1-\nu_i^2\right)}. \tag{4}$$

Y_i, Y_j, ν_i, ν_j, R_i, and R_j represent the Young's modulus, Poisson's ratio, and radii of spheres, respectively. The unit vector $\hat{n}_{ij}$, point toward granule j in the direction connecting

TABLE I. The material parameters [24,27,34].

Beads	Elastic modulus [GPa]	Poisson's ratio	Density [kg/m^3]	m_{striker} [g]
Tungsten carbide	628	0.28	14980	6.76
Stainless steel	200	0.28	7800	3.5
Aluminum	69	0.3	2740	1.2
PTFE	0.5	0.46	2200	0.9
Delrin	3.1	0.35	1400	0.6

the centers of granules i and j, and is given as

$$\hat{n}_{ij} = \frac{\mathbf{r}_j - \mathbf{r}_i}{|\mathbf{r}_j - \mathbf{r}_i|}. \tag{5}$$

Finally, $\mathbf{r}_i$ is the location vector of the center of particle i relative to the origin of the system at the center of the leftmost granule when $t = 0$.

A fourth-order Runge-Kutta method with time step $\Delta t = 10^{-8}$ s has been employed to integrate the Eq. (3). The accuracy of the method was tested by monitoring the conservation of mechanical energy and momentum. The relative errors were smaller than 10^{-12}, 10^{-14}, and 10^{-20} for the energy and the momentum in the x direction and y direction, respectively, across 10^5 time steps. In the next section we present our numerical results.

III. NUMERICAL RESULTS

We numerically integrated Eq. (3) using the material parameters presented in Table I.

The crystal was excited by the leftmost granule, which we call *the striker*. This granule is identical to those granules in the first layer. We consider the radii equal to $R = 4.76$ mm. The initial velocity of the striker was varied between 1 and 30 m/s. We observe the same dynamic behavior for both velocities, but in different time scales. For high velocities the wave propagation is faster. The results will be presented for 1 m/s, because this value is close to that in several experimental works [8,24,27]. We identify a specific direction along the crystal and call it the *secondary impact direction* (SID); see Fig. 1. The SID will be important to understand how we can control the way in which the wavefront spreads as it moves forward. By varying the radii of the granules, and hence the coordination number in the granular crystal, we can construct systems with the desired wave dispersion properties.

Crystals made with different material combinations are considered. We simulate systems where the main and the interstitial granules are made of different materials. To facilitate our discussion, we list the material combinations used in Table II. Each case is identified from 1 to 6. We focus on the outcomes for spherical granules, but it is easily possible to broaden our discussions to include the harmonic potential (cylindrical granules) as will be shown later. Therefore the present granular arrangement may be adapted for a different experimental setup. The wave attenuation is observed primarily due to differences in the elastic constants of the materials used and the system geometry that has been invoked.

The results are reported as follows. In Sec. III A, we discuss wave propagation in a bidisperse crystal; see Fig. 1(a). This case is an opportunity to: (i) check if our outcomes are in agreement with other works, (ii) analyze a good material combination to optimize the shock absorption, and (iii) compare the results when we consider the polydispersity. The numerical results for the tapered crystal, see Fig. 1(b), and comparisons with the bidisperse case are presented in Sec. III B. In Sec. III C, we comment on how the disorder in the radii affects the impact attenuation and what happens when the collision between the striker and the crystal is not head-on.

TABLE II. Material combinations analyzed are listed below. m_i/m_m is the approximate mass ratio of the interstitial and main granules.

Material combination	Main granules	Interstitial granules	m_i/m_m
Case 1	Tungsten	Delrin	0.006
Case 2	Stainless steel	PTFE	0.02
Case 3	Stainless steel	Stainless steel	0.071
Case 4	Aluminum	Stainless steel	0.202
Case 5	Delrin	Stainless steel	0.395
Case 6	Delrin	Tungsten	0.76

A. Granular crystal with bidispersity

In this section, we analyze a crystal where $q = 0$ [Eq. (1)]; see Fig. 1(a). The radii of interstitial granules are $r = R(\sqrt{2} - 1)$ and of the main granules are equal to R. This arrangement will be used as a reference scenario to inspect the influence of material combinations and for future discussions about the role of polydispersity ($q > 0$). Next, we will present a series of graphs to capture our findings on how the kinetic energy propagates through each of the material combinations listed in Table II. The dynamics for cases 1 to 6 are shown in Figs. 2 to 5. All crystals are made of 100-by-100 main granules (i.e., 99-by-99 central particles) with ~20 000 beads total.

In Figs. 2 to 5, there are some panels showing the same things in all cases. Panels (a) and (b) present snapshots for wavefront shapes when $t = 0.3$ and 0.9 ms, respectively. Panels (c(i)), (d(i)), and (e(i)) show the contour plots describing the propagation of the kinetic energy along the granules in specific directions, such as the SID and the chains bordering the impact direction. Along the same directions, panels (c(ii)), (d(ii)), and (e(ii)) show profiles of kinetic energy when $t =$ 0.3 and 0.9 ms. The insets in each panel identify, through a schematic arrangement, the granules under analysis (black circles).

Also, in Figs. 2 to 5 we observe the following basic dynamics. The striker collides with the crystal, imparting momentum and mechanical energy. The perturbation propagates like nonlinear waves. The wavefront shape and dynamics behind the leading wave are affected dramatically by the material parameters. The striker rebounds with a negative momentum (as we will discuss in Fig. 7). The energy spreads over the entire crystal attenuating the leading wave amplitude. We observe two simultaneous processes that are involved in the evolution of the wave: a part of the energy is distributed across a larger area, and another part ends up as secondary

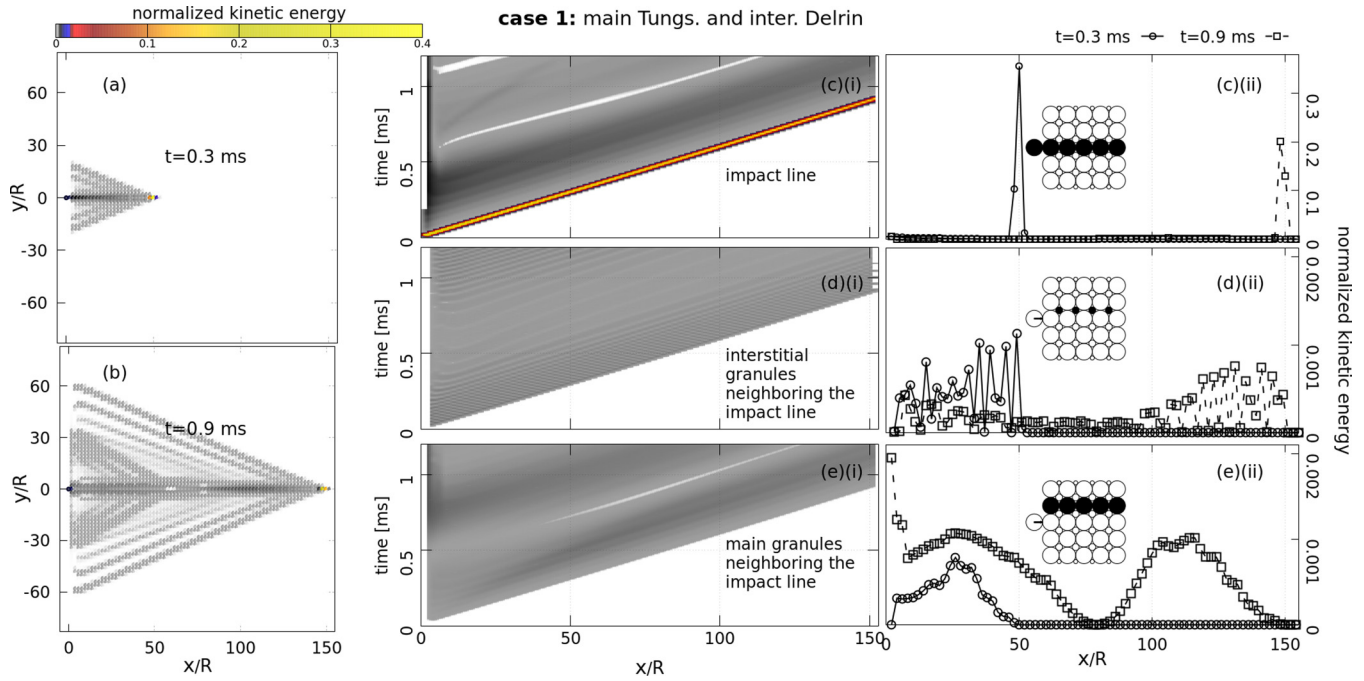

FIG. 2. Several panels show the evolution of kinetic energy in a bidisperse square crystal. The main and interstitial granules are made with tungsten and delrin, respectively. This material combination is identified as case 1. See comments regarding case 2 in the text. Snapshots at (a) 0.3 and (b) 0.9 ms show the energy along the whole crystal. The x and y axes represent the particle position. The distances are normalized by the radius of the largest sphere. The color scale indicates the normalized kinetic energy. Panels (c(i)), (d(i)), and (e(i)) are contour plots along specific granules. Profiles along the same specific granules at 0.3 and 0.9 ms are shown in panels (c(ii)), (d(ii)), and (e(ii)). Schematic diagrams highlight the granules under analysis (black circles). The energy propagates as a quasi-1D nonlinear wave.

waves with small amplitudes. The leading wave for each case is different, i.e., the dynamic-load-transfer phenomena depends on the materials involved. However, closer inspection reveals that some pairs of material compositions present similarities in dynamics and will be analyzed together.

Figure 2 depicts case 1, where in Figs. 2(a) and 2(b) we see the inability of the crystal to transfer tensile loads along the y direction and the propagation takes place mainly in line with the striker. Almost all the energy propagates along the impact line. Thus we call the leading wave supported for this case as quasi-1D nonlinear wave. Shukla *et al.* have conducted experimental investigations [21,22] using arrays of disks, with a geometry similar of Fig. 1(a) without interstitial granules. They had reported that the wave-propagation phenomenon is identical to that of a single chain and no energy was transferred to other chains. We see a comparable phenomenon in Fig. 2, because the main granules in the leading wave carry the energy. The interstitials granules carry almost no energy, due to the mass ratio (see Table II). Moreover, the load transfer produces secondary waves that propagates in diagonal directions [see Figs. 2(a) and 2(b)] which form triangular structures behind the leading wave. The origin of these structures lies in the fact that the wave propagation occurs through multiple collisions. The leading edge of the propagating wave has a width of several granules at any given instant of time. These granules first move forward, then the same granules move backward to collide with the interstitial granules located behind the wavefront. The load transfer paths for secondary waves in diagonal directions is related to the positions of interstitial granules in the arrangement.

In Fig. 2(c(i)), we observe the leading wave (colored line) followed by low-amplitude waves. The main and interstitial granules neighboring the impact direction also support waves with amplitudes very close to zero as shown in Figs. 2(d(i)) and 2(e(i)). A well defined pulse in line with the striker composed of five granules is presented in Fig. 2(c(ii)). For that pulse most of the energy is located in the three central granules. The pulse amplitude decays with the propagation distance. There are no pulses in other directions such as even in chains close to impact direction. For case 2 (see Table II) we also observed propagation as a quasi-1D nonlinear wave (not shown). The differences with respect to the previous case are that the leading wave has a lower amplitude and slower wave speed. More details will be discuss later, in Figs. 6 and 7.

The dynamic response for cases 3 and 4 are presented in Figs. 3 and 4, where we see in panels (a) and (b) that the wave propagation is characterized in two-dimension. We call the leading waves seen for these cases as two dimensional nonlinear waves. The dynamic load transfer for case 3 has an anisotropic characteristic. For that case the wavefront propagation is faster along the impact direction. For case 4 the dynamic load transfer becomes more isotropic and adopts an almost circular wavefront. Our results show that the mass ratio plays an important role in the shape of the wavefront (see Table II). Since the first few granules are compressed stronger against each other in these cases, more energy is transmitted through interstitial granular contacts when compared to cases 1 and 2. As a result, more energy propagates along the SID [see Fig. 1(a)]. This explains why the wavefront shape is completely different.

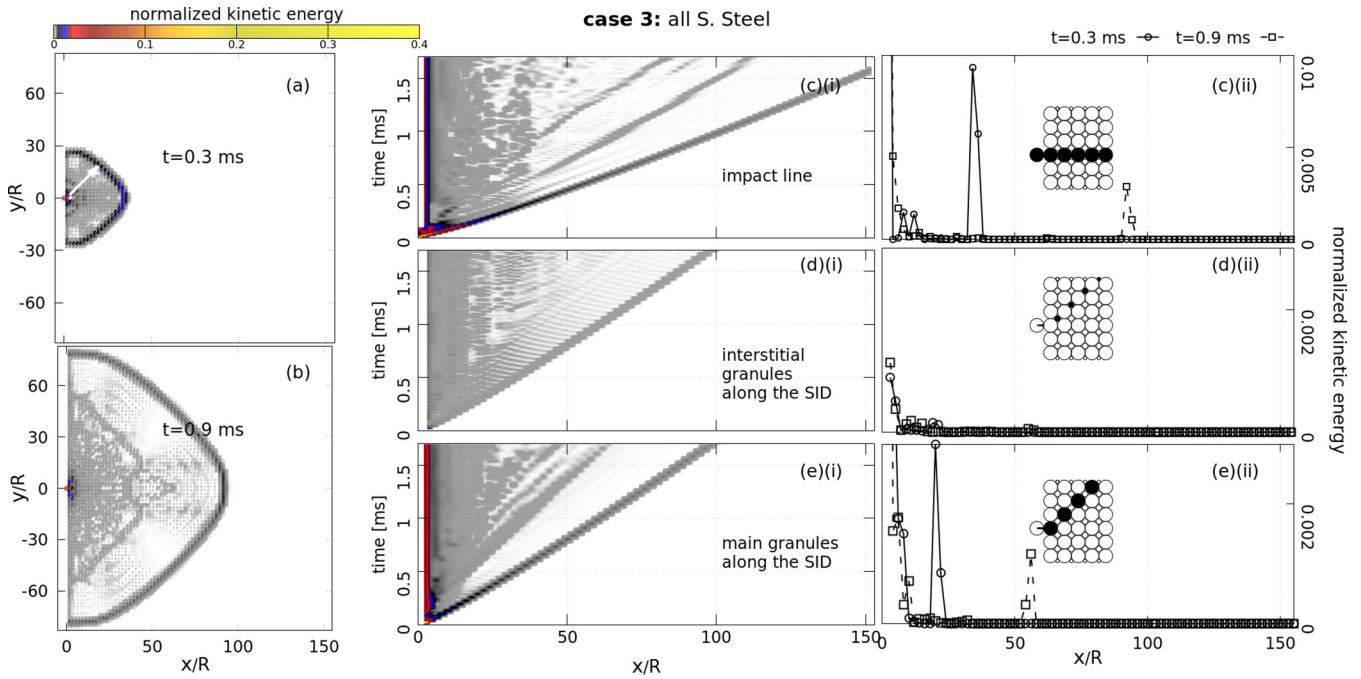

FIG. 3. Several panels show the evolution of kinetic energy in a bidisperse square crystal. All granules are made with stainless steal. This material combination is identified as case 3. Snapshots at (a) 0.3 and (b) 0.9 ms show the energy along the whole crystal. The x and y axes represent the particle position. The distances are normalized by the radius of the largest sphere. The color scale indicates the normalized kinetic energy. Panels (c(i)), (d(i)), and (e(i)) are contour plots along specific granules. Profiles along the same specific granules at 0.3 and 0.9 ms are shown in panels (c(ii)), (d(ii)), and (e(ii)). Schematic diagrams highlight the granules under analysis (black circles). The energy propagates as a 2D nonlinear wave.

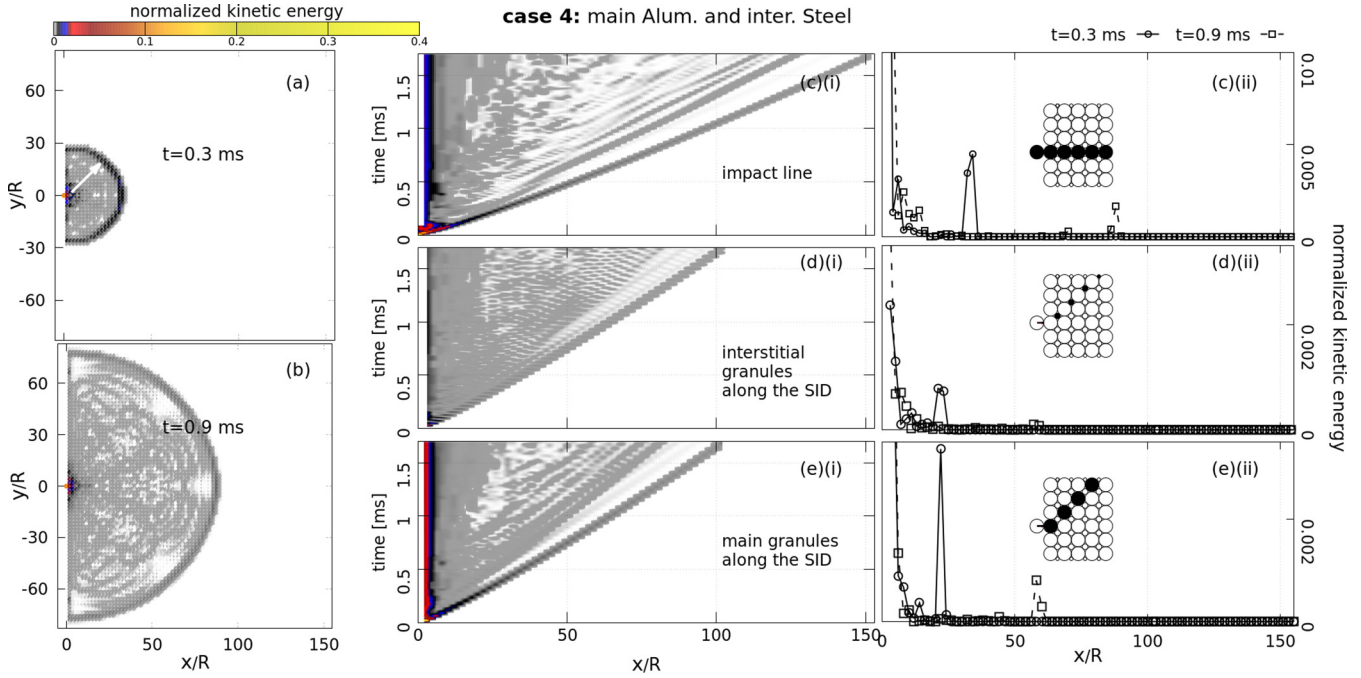

FIG. 4. Several panels show the evolution of kinetic energy in a bidisperse square crystal. The main and interstitial granules are made with aluminum and stainless steal, respectively. This material combination is identified as case 4. Snapshots at (a) 0.3 and (b) 0.9 ms show the energy along the whole crystal. The x and y axes represent the particle position. The distances are normalized by the radius of the largest sphere. The color scale indicates the normalized kinetic energy. Panels (c(i)), (d(i)), and (e(i)) are contour plots along specific granules. Profiles along the same specific granules at 0.3 and 0.9 ms are shown in panels (c(ii)), (d(ii)), and (e(ii)). Schematic diagrams highlight the granules under analysis (black circles). The energy propagates as a 2D nonlinear wave. The wavefront is almost circular.

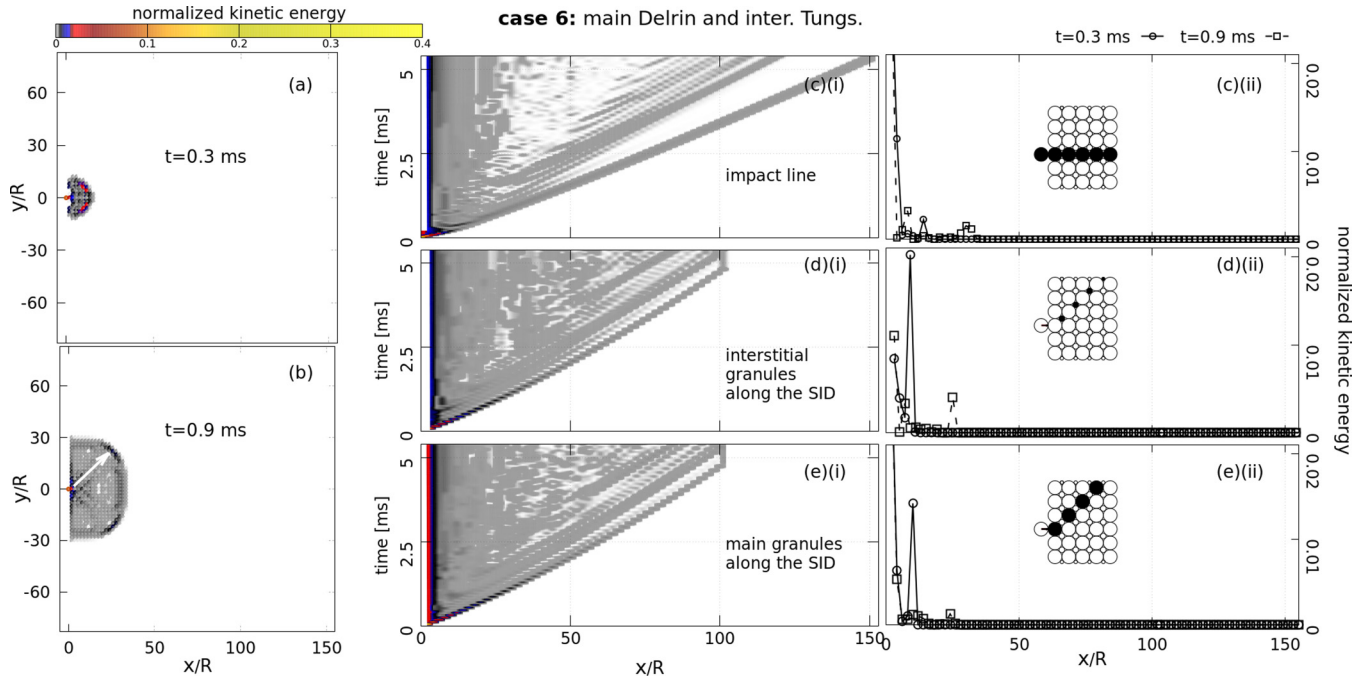

FIG. 5. Several panels show the evolution of kinetic energy in a bidisperse square crystal. The main and interstitial granules are made with delrin and tungsten, respectively. This material combination is identified as case 6. Snapshots at (a) 0.3 and (b) 0.9 ms show the energy along the whole crystal. The x and y axes represent the particle position. The distances are normalized by the radius of the largest sphere. The color scale indicates the normalized kinetic energy. Panels (c(i)), (d(i)), and (e(i)) are contour plots along specific granules. Profiles along the same specific granules at 0.3 and 0.9 ms are shown in panels (c(ii)), (d(ii)), and (e(ii)). Schematic diagrams highlight the granules under analysis (black circles). The energy propagates as a 2D nonlinear wave.

It can clearly be seen from panels (c(i)) of Figs. 3 and 4 that the leading wave's amplitude along the impact direction decreases rapidly after a few granules. The slope of the curve that identifies the leading wave increases with wave propagation. Consequently more time is needed to cover the same distance or number of layers. A similar behavior is observed in the SID as shown in panels (d(i)) and (e(i)) of Figs. 3 and 4. We see that the wave propagation is primarily supported by the main granules. A pulse with wavelength of five granules and decreasing amplitude with propagation distance is shown in panels (c(ii)) of Figs. 3 and 4. An analysis regarding the wave amplitude reveals that the role of interstitial granules is to spread the leading wave and the main granules is to support the wave propagation, as shown in panels (d(ii)) and (e(ii)) of Figs. 3 and 4.

Finally, the dynamic load transfer for case 6 is presented in Fig. 5, where we observe 2D nonlinear waves. When we compare with all previous cases, the case 6 carries more energy along the SID. This behavior allows highly effective shock dispersion. The same behavior was observed for case 5 with a similar wavefront shape (not shown). The differences are less energy along the SID, the leading wave with higher amplitude, and faster wave speed. Some details will be presented in Figs. 6 and 7. We analyzed the wavefront shapes from cases 1 to 6 and noted that the closer the mass ratio is to one (see Table II) slower is the wavefront speed, lower is the wavefront amplitude along the impact direction, and shorter is the propagation distance to attenuate the leading wave. Particularly, case 6 is the one that shows the mass ratio closest to one and it is more effective in redirecting the initial energy from impact line to the SID [see Fig. 5(b)].

We can analyze the energy dispersion measuring the wave propagation distance as a function of time as shown in Figs. 5(c(i)), 5(d(i)), and 5(e(i)). The slope of the curve corresponding to the wavefront increases with propagation

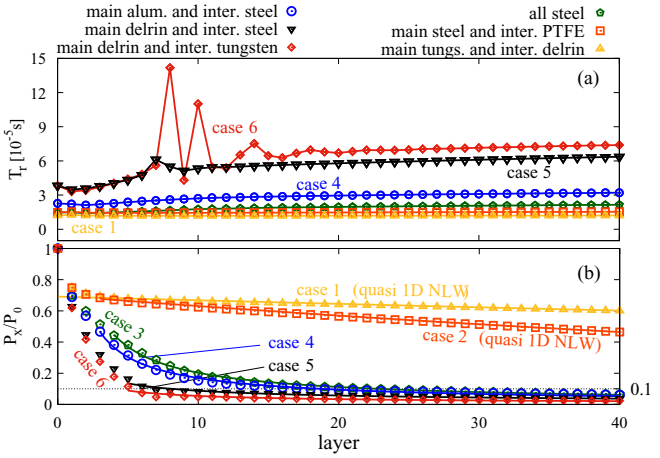

FIG. 6. Data for momentum wave propagation in line with the striker. (a) Residence time of the wave in each layer, where lines are guides to the eye. (b) Decay of the momentum wave amplitude as a function of layers, where the curves that best fit the data are described in Table III. Among the materials tested the best combination to attenuate impacts is the case 6; see Table II.

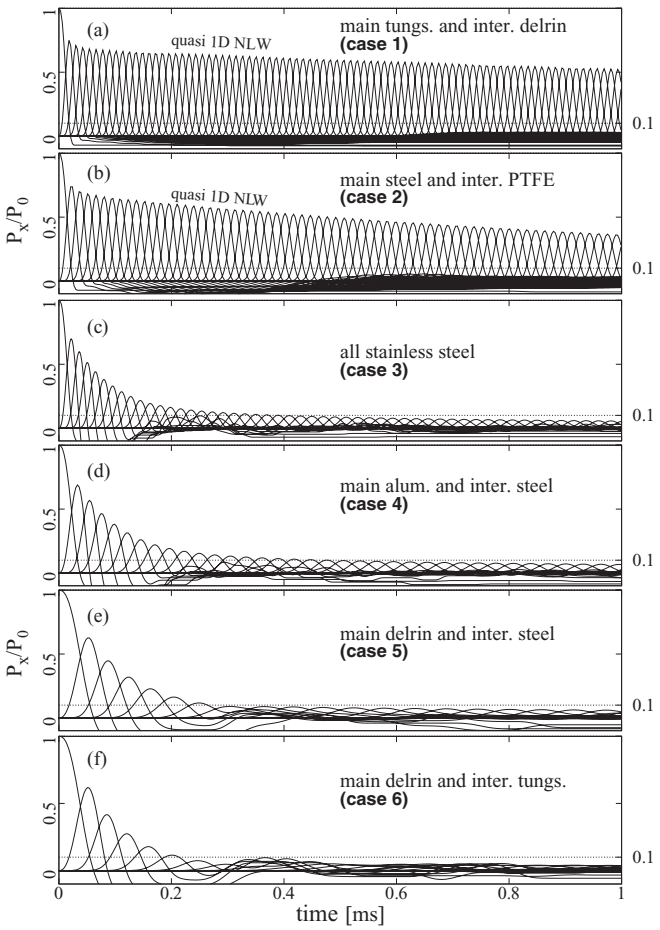

FIG. 7. Evolution of normalized momentum for each granule in-line with the impact direction. P_x is the x component of momentum (the same direction of impact). P_0 is the momentum of the striker. The decay of the amplitude is affected by the material parameters. There are secondary waves that surpass the wavefront for cases 5 and 6.

distance. The time for the wavefront to cover the same distance also increases. The interstitial particles change their roles to that of distributing energy to ever-larger areas to disperse the propagating energy. The energy profiles reveal the capacity of appropriate granular arrangements to attenuate disturbances using material combinations as in cases 5 and 6, shown in Figs. 5(c(ii)), 5(d(ii)), and 5(e(ii)). For these cases we see very low amplitudes after a short propagation distance. Regarding case 6, less than 1% of the initial energy is measured in the leading wave after a few layers. It is worth mentioning that the attenuation of wave amplitude in line with the striker is listed in increasing order from cases 1 to 6 [see panels (c(ii)) of Figs. 2–5]. More details about the wave characteristics along the impact direction will be discussed next.

Some previous studies that focused on the role of mass and stiffness (Young's modulus) in a centered square granular crystal reported similar results regarding the wavefront shapes [26–28]. Awasthi and co-workers have explained the existence of two propagation regimes. They have predicted theoretically both dynamics with a wave propagation map using kinematic and energetic arguments in Ref. [26]. We are calling these

TABLE III. The functional fit for the data in Fig. 6(b), where $l =$ layer. The constants are listed for each material combination.

Case	$f(l)$	a	b
1	ae^{-bl}	0.691317	0.00346807
2	ae^{-bl}	0.698735	0.0102147
3	al^{-b}	1.47445	0.860849
4	al^{-b}	1.17123	0.840328
5	al^{-b}	0.366767	0.621549
6	al^{-b}	0.271303	0.696246

regimes as quasi-one and two-dimensional nonlinear waves. Although the initial conditions described in Fig. 1(a) are different, the predictions are in good agreement with our results.

Figure 6 depicts the evolution of the normalized momentum pulse in line with the striker for the same material combinations presented in Table II. Two aspects are analyzed: Fig. 6(a) shows the residence time of the leading wave in each layer and Fig. 6(b) the decay of the momentum pulse amplitude as it travels along the crystal. Both are measured according to Ref. [11]. The momentum pulse arriving at layer l is that one when the momentum of layer l is greater than that of layer $l-1$. The residence time T_r in layer l is the time taken by the granule in layer l to transfer the wave from $l-1$ to $l+1$.

Figure 6(a) reveals that the residence time is highly influenced by the attenuation of wave amplitude. We can list the longest T_r in ascending order from cases 1 to 6. In fact, for one-dimensional systems and elastic waves, several studies have explored experimentally and analytically a relation between wave-speed and amplitude as $v \sim A^{\frac{1}{6}}$ [35–37]. It is expected in the present crystal that waves with high amplitude move faster than those with low amplitude. Thus, a steeper slope in T_r indicates a lower wave-speed. For cases 5 and 6, the small decay in the first layers represents that the leading wave is not well formed. After that point for cases 5 and 6, and at any given time for other cases, T_r increases slowly with the propagation distance. The phenomena that attract attention are abrupt variations in cases 5 and 6 of Fig. 6(a). These variations happen due to secondary waves with higher amplitudes that surpass the leading wave. In a scenario like that the behavior of residence time ends up not being smooth. The results in Fig. 7 will help to see the secondary waves.

The attenuation of the leading wave amplitude is very sensitive to material combination, see, e.g., the momentum decay presented in Fig. 6(b). The curves that best fit these results are described in Table III. When the granular arrangement supports the 2D nonlinear waves the improvement in impact absorption is remarkable compared to what is seen for quasi-1D nonlinear waves. The best attenuation results are obtained with cases 5 and 6. For these cases the incident momentum decreases to less than 10% after a few layers. Such noticeable attenuation is due to the interstitial granules. The attenuation is maximum when the masses of the interstitial granules are comparable to the masses of the main granules. Case 6 is an example; see Table II. Stronger collisions allow the heavier interstitial particles to redirect the characteristic load transfer path in line with the striker to the SID [Fig. 1(a)].

Figure 7 shows the evolution of normalized momentum profile for each granule in-line with the impact direction. Due to the impact event being in two dimensions and due to the appropriate material combination used, the momentum amplitude decays from slow to rapid for cases 1 through 6, respectively. The profile becomes wider with the propagation distance. This explains the longer residence times in each layer and a lower propagation velocity, as seen in Figs. 6(a) and 6(b), respectively. The overall effect of a wider profile with low amplitude is the dispersion of impacts. There are secondary pulses behind the wavefront with complicated dynamics in all cases. However, for cases 5 and 6 the leading wave amplitude decays dramatically in the first layers and it is almost completely attenuated. Thereafter the secondary waves with higher amplitudes exceed the wavefront. To see this observe in Fig. 6(a) the peaks in T_r around layer 10 (between 7 and 11, or so).

The analyses of all these results lead us to conclude that it is possible to direct the leading wave propagation in a decorated 2D granular crystal using material combinations in such a way that we could control the wave dispersion through the two processes: the formation of the wavefront shape and the scattering of energy behind the leading wave. These phenomena are responsible for explaining how the disturbance moves forward and why there are several secondary nonlinear waves.

Our simulations show that the wavefront shapes are strongly influenced by the presence of interstitial granules. The paths along the SID allow for more grain-grain collisions of the propagating excitation. However, there are limits to how much energy the granules in the SID can carry at any given time. With increasing impact energy we find that the granules are not able to transfer the incident energy into the crystal efficiently. As a result the pulse is broken into a leading front with secondary waves that follow.

The results suggest that the combination in case 6, has a more significant effect in the scattering of the wave and, consequently, in the wave dispersion. After a few layers ∼90% of the initial impulse is effectively dispersed. In spite of our calculations presented here, it is conceivable that using a suitable material combination with mass ratio closer to one and following the wave propagation map proposed in Ref. [26], one can find even better impact dispersion. In the next section, we continue exploring an optimal material combination. We will investigate if it is possible for the dispersion to be even greater when we include polydispersity in the crystal.

B. Granular crystal with polydispersity

In this section, we examine the dynamics in tapered crystals. We have made repeated attempts to sort out the maximum number of layers ($l_{\max}$) needed to avoid precompression as a function of tapering parameter q (see Fig. 8). For each value of q a granular crystal was built layer by layer, where in each step precompressions were investigated. The last layer was discarded when overlaps were observed. A power law behavior is clearly seen in the inset of Fig. 8, where we plot $l_{\max}$ versus q in log - log scale. The negative power is expected since an increase in the tapering parameter leads to faster tapering. A faster increase of the radii of interstitial granules also is observed as a consequence. We find that for

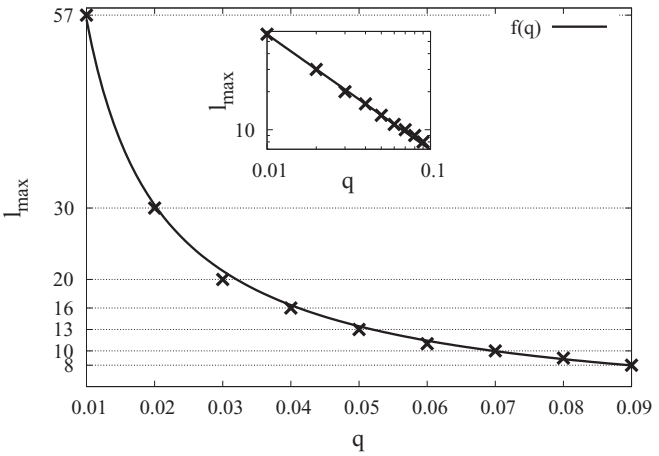

FIG. 8. Maximum number of layers in the crystal, to avoid precompression, as a function of the tapering parameter q. The curve that best fits the data is $f(q) = 0.843191q^{-0.914244}$.

$q \geqslant 0.07$ the crystals are quite short, about 10 layers long or less. Figure 9 shows the decay of the maximum momentum (wave amplitude) in line with the impact direction for several values of q. The same material combinations presented in Table II are used.

While the wave propagation remains sensitive to the material composition, the tapering contributes to enhancing the decay of the momentum. For example, while case 2 produced a ∼60% attenuation in momentum for all values of q, we are able to decrease the volume of the crystal from 20 layers for $q = 0.03$ to 8 layers when $q = 0.09$, as shown in Fig. 9. It is worth mentioning that the initial perturbation is almost completely attenuated even for those q values that produce very short crystals. We observe that the last granule behaves differently. There is an increase in its amplitude due to it being ejected from the crystal. The best outcomes are seen for case 6 and $q = 0.09$. For this crystal the momentum exhibits a very

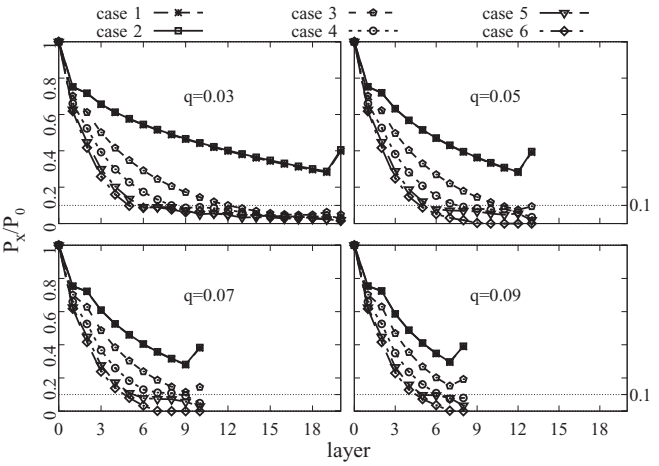

FIG. 9. Decay of momentum amplitude in line with striker for each tapering parameter. All cases are described in Table II. The crystals are as long as possible; see Fig. 8. The momentum is almost completely attenuated despite the very small number of layers. Lines are guides to the eye.

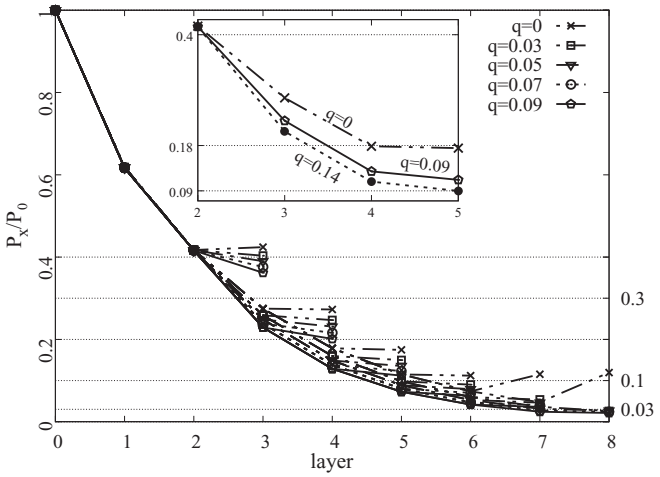

FIG. 10. Decay of momentum along the impact direction for crystals as case 6, see Table II. The numbers of layers are from 3 to 8, in steps of 1. The inset shows that with five layers the amplitude is reduced by ∼10% more when $q = 0.14$ than $q = 0$. Lines are guides to the eye.

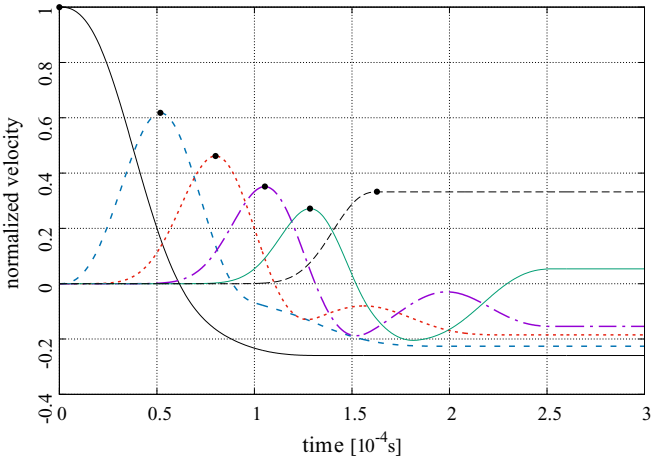

FIG. 11. Velocity profile as a function of time along the impact direction. The crystal is made with five layers, $q = 0.14$, and materials as case 6 (see Table II). There are no secondary waves and the last granule is ejected.

sharp decay with more than 90% of dispersion after only five layers. Such dramatic decay indicates that we do not need long crystals for impact dispersion in these systems. As the wave amplitude drops significantly in the first layers and the decay is more gradual after that, the granular arrangement could be shorter. We could build a crystal with very small number of layers and yet be able to mitigate impacts. The next step is to investigate how short the crystal would be. Henceforth, all results are reported using the material combination of case 6.

Figure 10 shows the decay of momentum along the impact direction for a variety of qs in the crystals with the number of layers from three to eight. The crystals are so short that the difference in behavior of internal granules is small, the exception is the last particle due to it being ejected. We find that only from layer 3 the effects of polydispersity become relevant. To understand the importance of layer 3, we note that this is where the interstitial and main granules possess comparable radii. From layer 3 onwards is where the momentum is redistributed to other directions from the impact line. The average momentum at the end of the crystal is at least reduced by ∼60% for crystals with three layers and almost completely attenuated for crystals with eight layers. For $q = 0.09$ and five layers the maximum momentum is reduced by ∼88%. However, the inset of Fig. 10 shows that for a crystal with five layers the maximum tapering parameter to avoid precompression is $q = 0.14$. This large q value may still be achievable because the crystal would be several layers. For this case, the peak of incident momentum is reduced by ∼91%. An improvement of ∼10% when compared to $q = 0$ (bidisperse crystal), see the inset in Fig. 10.

In Fig. 11 we show the evolution of the velocity profile for each of the main granules along the impact direction in a crystal with five layers and $q = 0.14$. As the crystal is short, there is no space to support secondary waves. The striker and some internal granules rebound with negative velocities. The initial perturbation is not completely transferred to each new layer and the amplitude decays rapidly. The last granule does not follow the decay pattern because it is ejected. The final amplitude is ∼30% of the input. When we compare the results of Figs. 10 and 11 we find that the decay of momentum is steeper than that in the velocity. This makes it clear that the mass dominates the momentum behavior in granular systems.

To understand the dynamics of our system, we investigate how the mechanical energy propagates from one layer to the next. Figures 12 and 13 show cases where the contacts are described by Hertzian and harmonic potentials, respectively. Panels (a) depict the mechanical energy propagation through each of the layers, where the insets show a typical sequence of 5 snapshots. The additional inset shows the wave profile along the last layer. Some of the profiles along chains composed of the main and interstitial granules are shown in panels (b(i)) to (f(i)) and (b(ii)) to (f(ii)), respectively. The chains under analysis are highlighted in black circles in each of the panel.

In both Figs. 12 and 13, we see the same basic dynamics. Panels (a) in both the figures reveal that the striker rebounds after collision with the first layer. The energy is gradually imparted from one layer to another. A portion of the energy remains in the striker and in each layer. Thus, the crystal is not able to transfer forward the entire incident energy. The series of snapshots shows that the wave spreads as it travels through the system as follows. The leading wave with low-amplitude reaches the last granule in line with the striker. A large amount of energy is redirected from the impact line to the SID. When the size of the interstitial and main granules are comparable (around layer 3), the crystal's ability to backscatter and transmit tensile loads in the y direction (orthogonal to the impact) are realized. Therefore, the wave profile suffers a fast spatiotemporal dispersion. There is a peak in the last granule along the SID of ∼4% of incident energy for the Hertzian potential, see the inset of Fig. 12(a). For the harmonic potential the peak is ∼3.5%, as shown in Fig. 13. The normalized mechanical energy carried by the tapered chain structures at various positions along the crystals are shown in panels (b(i)) to (f(ii)) for both the figures. More

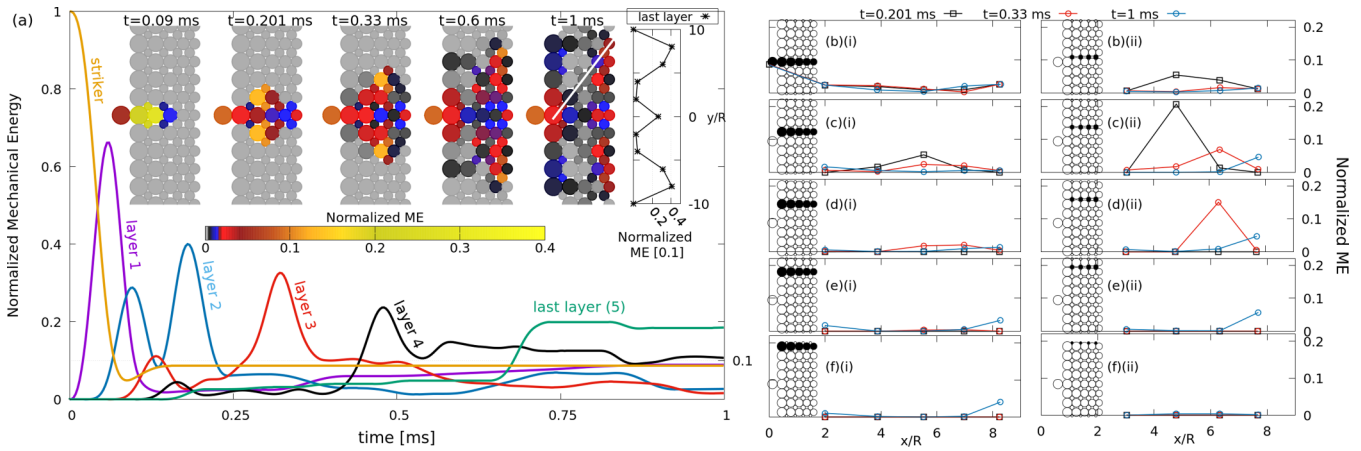

FIG. 12. Evolution of mechanical energy (ME) for a crystal with Hertzian contacts. The crystal is made with 5 layers, $q = 0.14$, and materials as case 6 (see Table II). (a) Profile for each layer. The insets depict snapshots of the wave. Additional inset shows the profile for the last layer at $t = 1$ ms. Profiles along chains composed of main granules are shown in panels (b(i)) to (f(i)). Profiles for interstitial granules are shown in panels (b(ii)) to (f(ii)). The chains under analysis are highlighted as black circles in schematic diagrams. A peak of 4% of incident energy is seen in the last granule along the SID.

energy travels through the interstitial granules than in the main granules, in both potentials.

The wave attenuation and dispersion for the harmonic potential is slightly more when compared to the Hertzian contact case. The difference is small due to the small number of layers that are present in the crystal. Particles under compression and interacting via linear forces support waves with wider profile and lower amplitude as function of propagation distance. As a consequence even monodisperse one-dimensional chains do not support stable solitary waves. This explains the absence of the central peak in the last layer for the harmonic potential, the different time scale, and the larger amount of energy redistributed in the first and last layers.

Next, we turn our attention for the role of disorder and not head-on collisions between striker and granules in the first layer.

C. Comment about disorder and not head-on collision

Last, we describe briefly the dynamics for two different initial conditions for the Hertzian contact problem. The scenarios considered are when the striker collides: (1) at the same time against two granules in the first layer, and (2) obliquely with only one granule. As expected, we note that the dynamics is comparable to that shown in Fig. 12 for both cases. We find that the striker rebounds and partially imparts its energy to the crystal. The energy transferred to the crystal rapidly attenuates as it travels through progressive layers. While the last layer is ejected, the perturbation is redirected from the impact line. There is a peak with small amplitude after only five layers along the SID. When the collision is not head-on the wavefront is no longer symmetrical.

To probe effects of weak positional disorder and small variation of radii, additional simulations were performed. It was

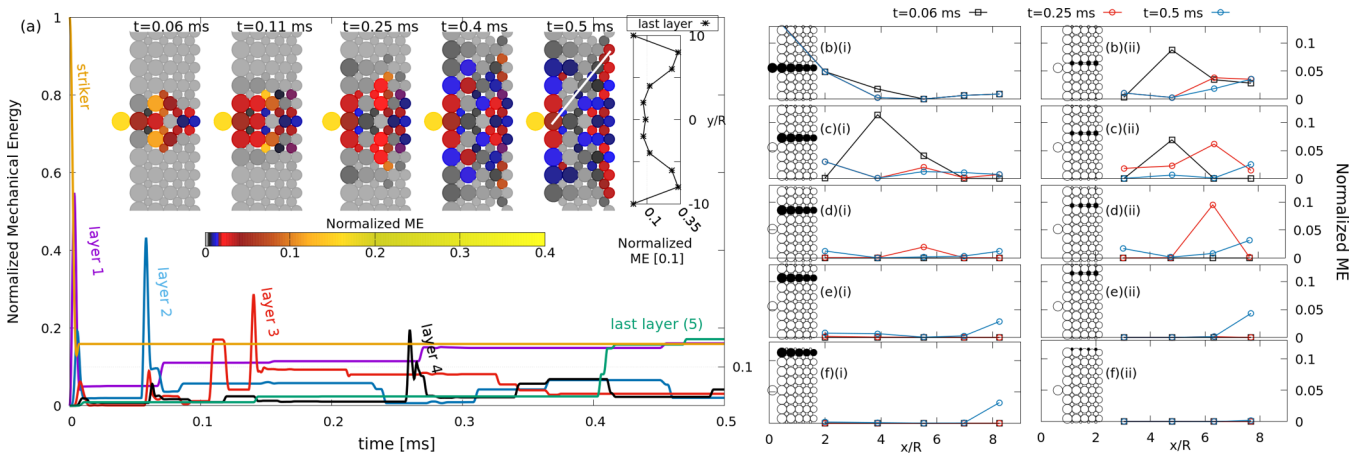

FIG. 13. Evolution of mechanical energy (ME) for a crystal with harmonic contacts. The crystal is made with 5 layers, $q = 0.14$, and materials as case 6 (see Table II). (a) Profile for each layer. The insets depict snapshots of the wave. Additional inset shows the profile for the last layer at $t = 0.5$ ms. Profiles along chains composed of main granules are shown in panels (b(i)) to (f(i)). Profiles for interstitial granules are shown in panels (b(ii)) to (f(ii)). The chains under analysis are highlighted as black circles in schematic diagrams. A peak of 3.5% of incident energy is seen in the last granule along the SID.

assigned for each granule a random radius where a variation of ±5% based on a normal distribution was allowed for the system. First, we used gravity along the impact direction to find the appropriate initial configuration of the system (i.e., without large precompressions or holes). Second, as there is always some residual kinetic energy in the system, we defined the initial positions of the granules as the average displacement. We have used that information to infer the approximate equilibrium positions. We measured the kinetic energy at the end of a crystal built with $q = 0.09$ and eight layers. The initial contact lattice affects the exact system response, but the initial energy imparted by a striker colliding head-on ended up being distributed along the last layer. The profile for the last layer is similar to Fig. 12.

IV. CONCLUSION

We have addressed the problem of impact dispersion in a tapered, ordered, square, granular crystal. The systems considered had two species of granules. The shape of the wave front was controlled by exploiting the geometry and the material combinations used to construct the granular crystal. We found that the right amount of tapering and the right combination of the two materials lead to severe impact attenuation within eight layers. Attenuation of incident momentum by ∼90% was noted for polydispersed systems 14% tapering. The impact attenuation in these tapered systems is an additional ∼10% less than that in the perfect crystals. Given that these systems have a limited number of layers, the effects of dissipation are small and have hence been ignored in the studies described here. Oblique as opposed to head on impact simply contributes to asymmetric dispersion of the propagating perturbation in the crystal. Further, small positional and geometric disorders have no significant influence on the impact dispersion of these tapered, bimodal, crystals.

In future studies we will discuss that the granular arrangement proposed here is also a good filter for continuous waves with $\sim 10^4$ and 10^5 Hz. The granular crystals considered here can be scaled down to spheres of $\sim 10^{-6}$ m and are able to support nonlinear granular breathing.

ACKNOWLEDGMENTS

The authors gratefully acknowledge financial support from the UFPA and logistic support from the SUNY-UB. L.P.M. also thanks the Department of Physics of UB for hospitality during his visit.

[1] S. Sen, J. Hong, J. Bang, E. Avalos, and Robert Doney, Phys. Rep. **462**, 21 (2008).
[2] M. Tiwari, T. R. K. Mohan, and S. Sen, Int. J. Mod. Phys. B **31**, 1742012 (2017).
[3] A. Rosas and K. Lindenberg, Int. J. Mod. Phys. B **31**, 1742016 (2017).
[4] U. Harbola, A. Rosas, A. H. Romero, M. Esposito, and K. Lindenberg, Phys. Rev. E **80**, 051302 (2009).
[5] R. Doney and S. Sen, Phys. Rev. Lett. **97**, 155502 (2006).
[6] R. L. Doney, J. H. Agui, and S. Sen, J. Appl. Phys. **106**, 064905 (2009).
[7] F. Melo, S. Job, F. Santibanez, and F. Tapia, Phys. Rev. E **73**, 041305 (2006).
[8] M. Nakagawa, J. H. Agui, D. T. Wu, and D. V. Extramiana, Granular Matter **4**, 167 (2003).
[9] R. L. Doney and S. Sen, Phys. Rev. E **72**, 041304 (2005).
[10] E. Braganca, A. Rosas, and K. Lindenberg, Physica A **392**, 6198 (2013).
[11] U. Harbola, A. Rosas, M. Esposito, and K. Lindenberg, Phys. Rev. E **80**, 031303 (2009).
[12] U. Harbola, A. Rosas, A. H. Romero, and K. Lindenberg, Phys. Rev. E **82**, 011306 (2010).
[13] L. P. Machado, A. Rosas, and K. Lindenberg, Granular Matter **15**, 735 (2013).
[14] S. Sen, F. S. Manciu, and M. Manciu, Physica A **299**, 551 (2001).
[15] L. P. Machado, A. Rosas, and K. Lindenberg, Eur. Phys. J. E **37**, 119 (2014).
[16] J. Hong and A. Xu, Appl. Phys. Lett. **81**, 4868 (2002).
[17] J. Hong, Phys. Rev. Lett. **94**, 108001 (2005).
[18] C. Daraio, V. F. Nesterenko, E. B. Herbold, and S. Jin, Phys. Rev. E **72**, 016603 (2005).
[19] C. Daraio, V. F. Nesterenko, E. B. Herbold, and S. Jin, Phys. Rev. Lett. **96**, 058002 (2006).
[20] A. Breindel, D. Sun, and S. Sen, Appl. Phys. Lett. **99**, 063510 (2011).
[21] A. Shukla and C. Damania, Exp. Mech. **27**, 268 (1987).
[22] A. Shukla, Optics and lasers in engineering **14**, 165 (1991).
[23] H. A. Burgoyne, J. A. Newman, W. C. Jackson, and C. Daraio, Procedia Eng. **103**, 52 (2015).
[24] C. Daraio, D. Ngo, V. F. Nesterenko, and F. Fraternali, Phys. Rev. E **82**, 036603 (2010).
[25] J. Yang, S. Dunatunga, and C. Daraio, Acta Mech. **223**, 549 (2012).
[26] A. P. Awasthi, K. J. Smith, P. H. Geubelle, and J. Lambros, Mech. Mater. **54**, 100 (2012).
[27] A. Leonard and C. Daraio, Phys. Rev. Lett. **108**, 214301 (2012).
[28] A. Leonard, C. Daraio, A. Awasthi, and P. Geubelle, Phys. Rev. E **86**, 031305 (2012).
[29] M. Nishida and Y. Tanaka, Granular Matter **12**, 357 (2010).
[30] M. Tiwari, T. R. K. Mohan, and S. Sen, Granular Matter **18**, 45 (2016).
[31] S. Sen, T. R. K. Mohan, and M. Tiwari, KONA Powder Part. J. **34**, 248 (2017).
[32] A. Sokolow, J. M. M. Pfannes, R. L. Doney, M. Nakagawa, J. H. Agui, and S. Sen, Appl. Phys. Lett. **87**, 254104 (2005).
[33] S. N. Ngoc and B. Brogliato, Granular Matter **14**, 341 (2012).
[34] E. Charalampidis, F. Li, C. Chong, J. Yang, and P. G. Kevrekidis, Math. Probl. Eng. **2015**, 830978 (2015).
[35] J. F. E. Richart, J. J. R. Hall, and R. D. Woods, *Vibrations of Soils and Foundations* (Prentice-Hall, Englewood Cliffs, NJ, 1970).
[36] J. D. Goddard, Proc. R. Soc. A **430**, 105 (1990).
[37] R. S. Sinkovits and S. Sen, Phys. Rev. Lett. **74**, 2686 (1995).